An Investigation into the Intrinsic Peroxidase-Like Activity of Fe-MOFs and Fe-MOFs/Polymer Composites

Bhawana Thakur,* Vikram V. Karve, Daniel T. Sun, A. Lisa Semrau, Lennart J. K. Weiß, Leroy Grob, Roland A. Fischer, Wendy L. Queen,* and Bernhard Wolfrum*

The quest for developing materials that provide a perfect trade-off between factors such as enzyme-like response, stability, and low cost has been a long-standing challenge in the field of biosensing. Metal-organic frameworks (MOFs) and their composites have emerged as promising candidates for biosensing applications due to their exceptional properties such as tunable pore size, high specific surface area, and exposed active sites. A comparative study of the intrinsic peroxidase-like activity of five different MOF materials: Fe-BTC, NH_2-MIL-101(Fe), composites of Fe-BTC with polymers polydopamine (PDA), poly p-phenylenediamine (PpPDA), and poly(3,4-ethylenedioxythiophene) is reported for the detection of H_2O_2, an important biomarker in biomedical diagnostics. The response of these materials toward H_2O_2 via electrochemical and colorimetric techniques is mapped and it is found that, at neutral pH, the Fe-BTC/PEDOT composite exhibits the highest sensitivity and activity compared to other MOF materials in this study. The results indicate that the combination of unique properties of Fe-BTC and conducting polymer PEDOT, improves the peroxidase-like activity of the Fe-BTC/PEDOT composite compared to the individual components. This work presents a new opportunity for easy-to synthesize and low-cost MOFs/conducting polymer composites for biosensing applications and provides significant insights to achieve rational design of composites with desirable functional properties

1. Introduction

Hydrogen peroxide (H_2O_2) is an important analyte in biomedical diagnostics. In human physiology, H_2O_2 acts as a biomarker for oxidative stress, which can be associated with medical disorders such as Alzheimer's disease, Parkinson's disease, myocardial infarction, and cancer.[1,2] Additionally, biosensors based on oxidase enzymes for detection of analytes such as glucose, uric acid, and neurotransmitters rely on monitoring the concentration of H_2O_2, which is generated during the enzymatic reactions.[3,4] Biosensors for the detection of H_2O_2 predominantly operate on optical and or electrochemical techniques and employ the peroxidase enzyme horseradish peroxidase (HRP). Although HRP-based biosensors offer high selectivity and sensitivity for H_2O_2 detection, factors such as high cost, short shelf life, and environmental instability limits their performance for wider applications.[2] This has led to numerous studies wherein alternative non-enzymatic entities known as peroxidase mimics, which possess intrinsic peroxidase-like catalytic activity for H_2O_2 detection, are explored for biosensing application.[5,6] To date, several classes of materials, such as noble metal nanoparticles, metal oxide nanoparticles, carbon-based nanomaterials, and transition metal complexes are known to mimic peroxidase activity.[5,7]

Of the many materials to select from, metal-organic frameworks (MOFs) are the latest addition to the pool of materials, which serve as peroxidase mimics, and several MOFs have displayed quite promising performance in this context.[8–12] Due to a number of attractive properties such as tunable pore size, high specific surface area, and large numbers of exposed active sites, MOFs are increasingly studied in biosensing applications. Within a biosensor, MOFs can act as a redox mediator and also encapsulate the biorecognition element.[13,14] Additionally, there is a possibility to introduce various functional groups within a given MOF structure promoting selectivity. For example, MOFs can be combined with metal nanoparticles, polymers, graphene, and carbon nanotubes (CNTs) for the production of a variety of interesting composites, which exhibit functionality that is not inherent to the pristine MOF itself. In particular, the recent integration of MOFs with polymers has given rise to a new class of composite materials with broader practical applications

Dr. B. Thakur, L. J. K. Weiß, L. Grob, Prof. B. Wolfrum
Neuroelectronics
Department of Electrical and Computer Engineering
Munich School of Bioengineering
Technical University of Munich
Boltzmannstraße 11, 85748 Garching, Germany
E-mail: bhawana.thakur@roche.com; bernhard.wolfrum@tum.de

V. V. Karve, Dr. D. T. Sun, Prof. W. L. Queen
Institute of Chemical Sciences and Engineering
Ecole Polytechnique Fédérale de Lausanne (EPFL)
EPFL-ISIC-Valais
Sion 1950, Switzerland
E-mail: wendy.queen@epfl.ch

A. L. Semrau, Prof. R. A. Fischer
Chair of Inorganic and Metal-Organic Chemistry
Department of Chemistry
Technical University of Munich
Lichtenbergstraße 4, D-85748 Garching, Germany

The ORCID identification number(s) for the author(s) of this article can be found under https://doi.org/10.1002/admt.202001048.

due to attractive properties including improved processability, conductivity, selectivity toward molecules, chemical and colloidal stability, and biocompatibility.[15–18] For instance, a recent study demonstrated that surface coatings consisting of a chemically modified polydopamine can improve the stability of a series of structurally diverse MOFs by inhibiting their hydrolysis and decomposition under extreme pH conditions.[19]

While improving the structural and chemical stability of MOFs is crucial for most general applications, making MOFs conductive provides a specific scope for their application in electrocatalysis, chemiresistive/electrochemical sensing, and energy storage technologies.[20] The majority of MOFs in their pristine form are insulating. However, integration of MOFs with materials such as CNTs, graphene, metal nanoparticles, and conducting polymers is becoming a common strategy to improve the electrocatalytic activity of a given framework.[21–23] For instance, there are several examples where conducting polymers, such as PEDOT, were successfully integrated within MOFs, improving the electronic conductivity when compared to the parent material.[24–27] In addition to conductivity, there are several recent examples of MOFs and MOF-composites, which have exhibited intrinsic peroxidase-like activity for H_2O_2 detection,[8,28–31] providing a strong case for the use of MOFs in biosensing applications. However, when looking at the volume of published articles, very few reports to date have conducted systematic studies to understand structure–function correlations for MOFs or MOF–polymer composites in such applications.[10,32] These types of studies are important for the rational design of porous materials that offer properties necessary for their implementation in different sensing applications.

In the current work, we have investigated the artificial peroxidase-like activity of two Fe-based MOFs materials namely Fe-BTC (Basolite300) and NH₂-MIL-101(Fe), as well as polymer composites of Fe-BTC containing polydopamine (PDA), poly p-phenylenediamine (PpPDA), and poly(3,4-ethylenedioxythiophene) (PEDOT). It is noted that the selected polymers are already frequently used in the fabrication of biosensors because their incorporation into the matrix of a transducer is known to enhance various properties of the device.[4,33–36] For instance, many wearable biosensors are fabricated using PDA, which mimics muscle foot proteins, imparting a strong adhesive property and offering biocompatibility.[37,38] Additionally, the presence of catechol groups in PDA and –NH₂ functionality in PpPDA facilitates the covalent immobilization of biorecognition elements during the fabrication of biosensors.[36,39] Further, apart from the excellent conductivity, PEDOT is also biocompatible, which makes it an ideal candidate for in-vivo sensing applications.[40–42]

Since iron exhibits low toxicity and high biocompatibility, we selected two low-cost and easy to synthesize Fe-MOFs in our study.[43,44] The first MOF, Fe-BTC, comprises $Fe_3(\mu_3\text{-}O)$ building units with 1,3,5-benzenetricarboxylic acid (BTC) linkers. Due to its high catalytic activity for a variety of organic transformations, this material has been extensively explored for various applications in catalysis/photocatalysis, sensing, and environmental remediation.[44–46] The second Fe-MOF used in this study is NH₂-MIL-101(Fe) also consists of $Fe_3(\mu_3\text{-}O)$ building units linked by a 2-aminoterephtate linker. NH₂-MIL-101(Fe) exhibits low toxicity, which makes it attractive for in vivo activi-

ties such as drug delivery and in situ imaging.[43] Further, the presence of amine groups in NH₂-MIL-101(Fe) provides the possibility for its post-synthetic modification with various biomolecules.[47,48] After the synthesis of the MOFs, Fe-BTC was subsequently infused with several polymers, including PDA, PpPDA, and PEDOT using pre-established procedures for post-synthetic polymerization.[16,49] The reactivity of the synthesized materials with H_2O_2 was studied using cyclic voltammetry and UV-vis spectrophotometry. Prior to the sensing experiments, the size and morphological properties of the synthesized MOFs were verified with the help of characterization techniques such as scanning electron microscopy (SEM), N_2 adsorption, and powder X-ray diffraction (XRD).

2. Results and Discussion

2.1. Characterization

Fe-BTC and NH₂-MIL-101(Fe) were synthesized using previously reported procedures.[50] Three polymers, namely PDA, PpPDA, and PEDOT were inserted into Fe-BTC using known strategies for post-synthetic polymerization, which allows the growth of the polymer chains inside a given MOF structure.[16,49] During polymerization, the corresponding monomers, i.e., dopamine, p-phenylenediamine, and 3,4-ethylenediethoxythiophene diffuse into the pores of Fe-BTC and subsequently undergo polymerization via an anaerobic oxidation process. Similar to the classical method for the synthesis of conjugated polymers, wherein Fe^{+3} is often employed as the oxidant, the synthesis of Fe-BTC/polymer composites proceeds with the reduction of Fe^{3+} to Fe^{2+} followed by the oxidation of the amine group/hydroxyl group/thiophene ring in the corresponding monomer.[51,52] Polymerization of monomers within the cavities of Fe-BTC is apparent from the N_2 adsorption isotherms, where the BET surface area of Fe-BTC/polymer is reduced by 50% when compared to the pristine Fe-BTC (Figure S1 and Table S1, Supporting Information). Further, the Fe-BTC undergoes a color change from light orange to a dark color due to the presence of the highly conjugated polymers. Nonetheless, the Fe-BTC/polymer composite has a considerable amount of residual porosity, which provides room to embed additional materials such as nanoparticles, and enzymes to expand the application scope toward biosensing. In previous studies, it was shown that the guest polymers are pinned inside the MOF structure and hence remain confined within the pores of MOFs after soaking in solution.[16,49] Thus, it was expected that the structural integrity of Fe-BTC/polymer composites could be maintained over the course of electrochemical and optical measurements, which were carried out in phosphate buffer saline (PBS, pH 7.4). Further, similar to previous reports the SEM images of Fe-BTC/polymer composite did not show any polymer formation on the external MOF surface (Figure S2, Supporting Information).[16,49] In addition to this, SEM images of NH₂-MIL-101(Fe) reveal a hexagonal microspindle morphology with crystal lengths that range from 1 to 2 µm and widths between 0.5 and 1 µm. Further, the crystallinity of the Fe-BTC structure is maintained after polymerization as evident from their XRD patterns, which match well with the simulated XRD pattern of Fe-BTC (Figure S3, Supporting

ADVANCED
SCIENCE NEWS
www.advancedsciencenews.com

ADVANCED
MATERIALS
TECHNOLOGIES
www.advmattechnol.de

Information). As in the case of Fe-BTC, the XRD pattern of NH_2-MIL-101(Fe) matches well with the simulated pattern of the isostructural MIL-101 (Cr) analog (CCDC 605 510), which was used as a reference. Since the Fe-BTC/PEDOT composite exhibited the best sensing performance among the MOFs and MOF/polymer composites used in this study, XRD patterns of Fe-BTC and Fe-BTC/PEDOT were recorded before and after exposure to PBS and H_2O_2 to investigate the stability of these materials. The XRD patterns did not show any notable change when Fe-BTC and Fe-BTC/PEDOT was subjected to PBS and various concentrations of H_2O_2, which indicates good stability and structural integrity of these materials during the sensing measurements (Figure S4, Supporting Information).

2.2. Electrochemical Study

The widely accepted mechanism for the catalytic decomposition of H_2O_2 in presence of ferrous (Fe^{+2}) and ferric (Fe^{+3}) ions is based on the classical Haber Weiss mechanism/Fenton-type reaction, which propose the formation of reactive hydroxyl radical ($HO^{\bullet}$).[53–56] While Fe^{+2} is more reactive toward H_2O_2 in the pH range of 3–4, Fe^{+3} has a fair reactivity with H_2O_2 under neutral pH conditions. Furthermore, a study on reactivity of Fe^{+3} ions revealed that a coordinated Fe^{+3} ion is a more efficient catalyst for decomposition of H_2O_2 compared to free Fe^{+3} ion at neutral pH.[55,57] Since many of the physiological processes occur at pH ≈7.4, we narrowed the scope of our studies for the sensing performance of MOFs at neutral pH. Although H_2O_2 can be detected electrochemically by oxidation or reduction, the application of a reduction potential minimizes interference and improves selectivity of the sensor.[58] Electrodes modified with materials containing transition metals such as Fe can exhibit peroxidase like activity, which offer the advantage of

low working potentials.[59] Several iron-based materials such as Prussian blue, magnetic nanoparticles, and very recently Fe-MOFs have been explored for development of biosensors with low operational voltage.[60–62] The mechanism for the electroreduction of H_2O_2 by iron-based materials is not well established and very few studies have been carried out in this direction.[59,63] In the case of iron-based materials, the electrocatalysis of H_2O_2 usually proceeds by electroreduction of Fe^{+3} to Fe^{+2} under the applied reduction potential, followed by oxidation of electrogenerated Fe^{+2} to Fe^{+3} by H_2O_2. Based on these reports, we propose the following electrochemical mechanism in aqueous media for the Fe-MOFs based materials used in this study.[53,59,64]

$$Fe^{3+} + e^- \rightarrow Fe^{2+} \tag{1}$$

$$Fe^{2+} + H_2O_2 \rightarrow Fe^{3+} + HO^- + HO^{\bullet} \tag{2}$$

$$HO^{\bullet} + e^- \rightarrow HO^- \tag{3}$$

$$HO^- + H^+ \rightleftharpoons H_2O \tag{4}$$

Figures 1 and **2** show the electrochemical response of Fe-MOFs and their polymer hybrids on carbon SPE with increasing concentration of H_2O_2. With the addition of H_2O_2, a concomitant increase in reduction current was observed in the CV of the MOFs materials. **Table 1** summarizes the overall performance of SPE modified with MOFs and MOF/polymer composites with respect to sensitivity, linear range, and detection limit for detection of H_2O_2. Among the five MOFs materials used for electrochemical detection of H_2O_2 in our study, the performance with respect to sensitivity was observed in the following order: Fe-BTC/PEDOT > Fe-BTC > Fe-BTC/PDA > Fe-BTC/PpPDA > NH_2-MIL-101(Fe). The limits of detection
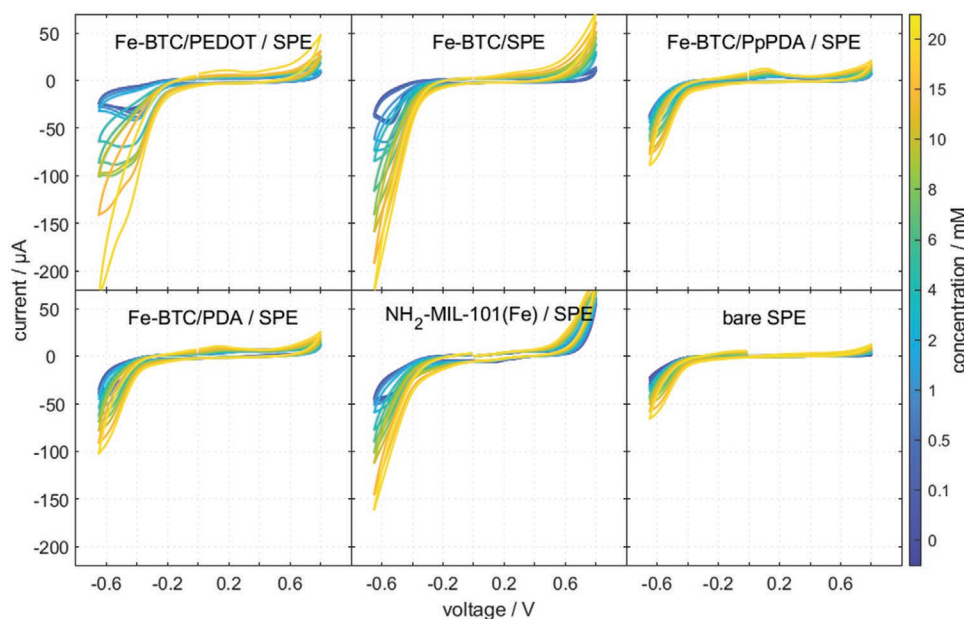

Figure 1. Cyclic voltammograms obtained with different SPE: Fe-BTC/PEDOT/SPE, Fe-BTC/SPE, Fe-BTC/PpPDA/SPE, Fe-BTC/PDA/SPE, NH_2-MIL-101(Fe)/SPE, and a bare SPE with increasing concentration of H_2O_2 (0 to 20×10^{-3} M) in PBS (pH 7.4). Scan rate: 50 mVs^{-1}.
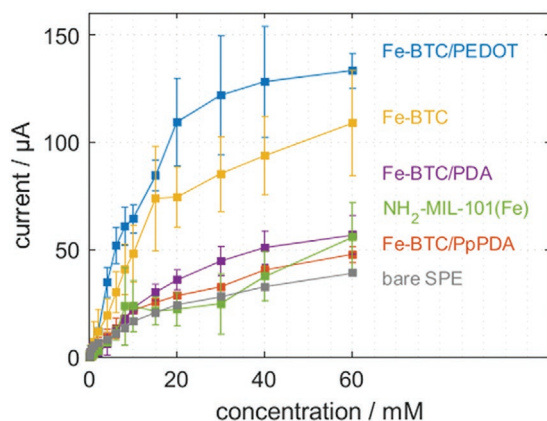
Figure 2. Response of a) Fe-BTC/PEDOT/SPE, b) Fe-BTC/SPE, c) Fe-BTC/PpPDA/SPE, d) Fe-BTC/PDA/SPE, e) NH_2-MIL-101(Fe)/SPE, and f) bare SPE with increasing concentration of H_2O_2 in PBS (pH 7.4). Plot derived from cyclic voltammetry data at applied potential of −0.5 V. Scan rate: 50 mVs^{-1}.

(LOD) of the sensor electrodes were calculated according to the 3σ criterion, where σ is the standard deviation for the blank measurements (without addition of analyte) ($n = 3$). The MOFs and MOF/polymer composites did not display exceptional LOD values compared to other H_2O_2 sensors based on materials such as metal nanoparticles, graphene, and CNTs. However, scaling down the working area of the electrode could provide an effective strategy to improve the detection limit of the sensors.[65,66] With respect to sensitivity, the performance of pristine Fe-BTC toward H_2O_2 sensing was either comparable or higher than some of the MOF-based materials reported in literature (see Table S2, Supporting Information).[30,67] In particular, the sensitivity of the Fe-BTC/PEDOT composite was almost two times higher than the sensitivity of pristine Fe-BTC, which can be attributed to the presence of PEDOT within the pores of Fe-BTC. In general, the intrinsic conductivity of PEDOT is known to improve the overall conductivity of composite materials.[68,69] The presence of conducting polymers improves the effective charge transfer within the MOF-based composites, which enhances its catalytic activity.[70,71] To estimate the con-

tribution of PEDOT in the Fe-BTC/PEDOT composite, we conducted a parallel study with bare PEDOT/SPEs for detection of H_2O_2 (Figure S6, Supporting Information). Compared to Fe-BTC/PEDOT, PEDOT exhibits significantly lower reduction currents for H_2O_2 sensing. Thus, we attribute the electrocatalytic reduction of H_2O_2 to the presence of Fe^{+3} centers in the Fe-BTC/PEDOT composite. The synergistic effect between Fe-BTC and PEDOT further enhances the performance of the composite for H_2O_2 sensing. A similar effect was observed in a PEDOT based MOF composite, which was synthesized for dopamine sensing. Here, PEDOT nanotubes served as charge collectors for efficient electron transport within the composite that consisted of electroactive porphyrin-based metal–organic framework nanocrystals (MOF-525).[68] Overall, the synergy between conductive polymers and MOFs has been explored in the context of potential electrocatalysis applications.[72]

For the Fe-BTC/PpPDA, the composites' sensitivity for the detection of H_2O_2 was reduced to half of the sensitivity of Fe-BTC. Also, despite that the selected polymer is a structural analogue of polyaniline, a highly conductive polymer, PpPDA unfortunately offers a relatively low conductivity of 10^{-7} S m^{-1}. It is thought that this low intrinsic conductivity could inhibit the catalytic activation of H_2O_2 on the surface of the electrode. Thus, PpPDA failed to maintain the redox activity of Fe-BTC. A similar decrease in sensitivity was observed for the Fe-BTC/PDA composite. It must be noted that PDA possesses poor electrical conductivity and furthermore is an excellent radical scavenging material.[73–76] Since hydroxyl radicals are produced during electrochemical redox reaction of H_2O_2, a radical scavenging component like PDA can heavily influence the chain-reaction type redox cycle of H_2O_2. The electrochemical impedance (EIS) studies were also carried out to assess the effect of polymers on the electrochemical activity of the Fe-BTC/polymer composites. The charge transfer resistance (R_{ct}) values were derived from the fitted values of the Nyquist plots in 1×10^{-3} M Fe(CN)$_6^{3-/4-}$ solution, which presents a Faradaic system (Figure S7, Supporting Information). The Nyquist plot consists of a diffusion-controlled section at lower frequency that is related to the Warburg impedance, and a semicircle region at higher frequency that is related to the parallel circuit of R_{ct} and the constant phase element.[77] The R_{ct} values of the composites were in the order as follows ($n = 3$): Fe-BTC/PEDOT (6.65 kΩ) < Fe-BTC (7.89 kΩ) < Fe-BTC/PpPDA (8.82 kΩ) < Fe-BTC/PDA (17.50 kΩ). Among the three different composites, Fe-BTC/PEDOT exhibited the lowest R_{ct} value. Overall, based on the results of the electrochemical studies it can be concluded that out of PEDOT, PpPDA, and PDA, only the PEDOT based Fe-BTC composite exhibited improved performance as a peroxidase mimic enzyme for detection of H_2O_2 under neutral conditions.

Further, in comparison with the peroxidase-like activity of Fe-BTC the electrochemical study revealed a very low activity of NH_2-MIL-101(Fe) for the detection of H_2O_2. The ligand of Fe-BTC comprises three carboxylic acid groups (−COOH) on the benzene ring whereas the ligand of NH_2-MIL-101(Fe) has two carboxylic acid and one amine (−NH_2) group on the benzene ring. In MOFs, the nature of functional groups on the ligand can increase or decrease the net charge on the central metal atom.[78] It is postulated that in the case of Fe^{+3}/Fe^{+2} system, the Fenton-type reaction is preceded by initial binding of H_2O_2 with Fe center to form an iron–peroxo complex.[56] In

Table 1. Electrochemical detection of H_2O_2: Summary of the analytical performance of SPE modified with metal-organic frameworks (MOFs) and MOFs/polymer composites for the detection of H_2O_2. The linear range, sensitivity, and limit of detection (LOD) were derived from the individual sensor responses (Figure 2 and Figure S5, Supporting Information).

MOFs/ MOFs composite	Linear range [× 10^{-3} M]	LOD [× 10^{-3} M]	Sensitivity [μA × 10^{-3} M^{-1} cm^{-2}]
Fe-BTC/PEDOT	0.5–6	0.46	73.89
Fe-BTC	0.5–8	0.41	37.42
Fe-BTC/PDA	2–10	1.17	20.94
Fe-BTC/PpPDA	0.5–10	0.45	16.88
NH_2-MIL-101(Fe)	1–6	0.63	15.76
SPE[a]	0.1–15	9.03*	1.49

[a]Unmodified SPE exhibited very high standard deviation (σ) value for the blank measurements, hence had a high LOD for H_2O_2.
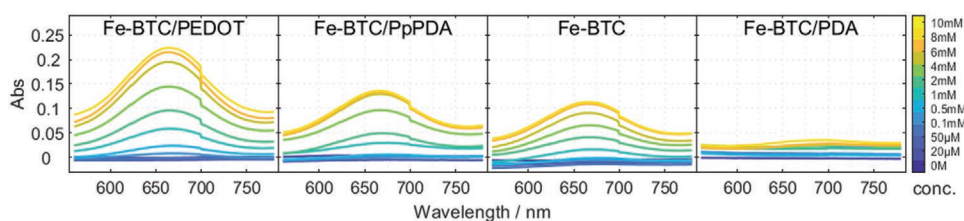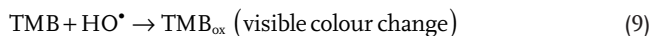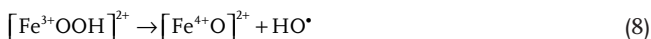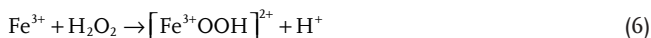
Figure 3. UV-vis spectra of Fe-BTC/PEDOT, Fe-BTC/PpPDA, Fe-BTC, and Fe-BTC/PDA with addition of H_2O_2 (0 to 10×10^{-3} M) in PBS (pH 7.4).

the current work, the presence of $-NH_2$, an electron-donating group could decrease the electrophilicity of the Fe cluster in NH_2-MIL-101(Fe) and reduce its affinity to H_2O_2. A similar observation was reported in a recent study where Cu-MOFs with ligands having $-NO_2$ group (electron acceptor) exhibited higher activity for the detection of H_2O_2 compared to Cu-MOFs with ligands having $-CH_3$, $-OH$, and $-NH_2$ groups (electron donors).[9] Moreover, varying the functional groups on a given ligand, can also have profound effects on the MOF topology, gas absorption property, and flexibility.[79–81] In addition to the nature of functional groups, porosity is another important factor, which dictates the activity of catalyst materials. Since, the pore dimensions of Fe-BTC (22 Å) and NH_2-MIL-101(Fe) (12 Å × 29 Å; 16 Å × 34 Å) are dissimilar to each other, the variation in their sensitivities could also be attributed to the differences in their porosity.[44,82] However, additional investigations into how the structure of these MOFs influences performance, can provide more insight into the higher sensitivity of Fe-BTC over that of NH_2-MIL-101(Fe) for the electroreduction of H_2O_2.

2.3. Optical Study

The intrinsic peroxidase-like activity of MOFs and their polymer composites was analyzed in presence of 3,3′,5,5′-tetramethybenzidine (TMB). The hydroxyl radicals formed during this Fenton-type reaction oxidize TMB, a chromogenic dye. The following redox mechanism is proposed for optical detection of H_2O_2.[54,64]

$$Fe^{2+} + H_2O_2 \rightarrow Fe^{3+} + HO^- + HO^\bullet \tag{5}$$

$$Fe^{3+} + H_2O_2 \rightarrow \left[Fe^{3+}OOH\right]^{2+} + H^+ \tag{6}$$

$$\left[Fe^{3+}OOH\right]^{2+} \rightarrow Fe^{2+} + HOO^\bullet \tag{7}$$

$$\left[Fe^{3+}OOH\right]^{2+} \rightarrow \left[Fe^{4+}O\right]^{2+} + HO^\bullet \tag{8}$$

$$TMB + HO^\bullet \rightarrow TMB_{ox} \left(\text{visible colour change}\right) \tag{9}$$

The peroxidase activity was marked by a gradual rise of absorption peak at 652 nm after the addition of H_2O_2 to a solution of TMB and MOFs/MOFs-polymer composites (**Figure 3**). The result is in accordance with previous reports on Fe-based artificial peroxidase enzymes. We also studied the effect of pH on the peroxidase-like activity of MOFs/MOFs-polymer composites (Figure S8, Supporting Information). Unlike Fe-BTC/PDA and NH_2-MIL-101(Fe), wherein the peroxidase-like activity for 0.5×10^{-3} M H_2O_2 dropped to ≈0%, Fe-BTC/PEDOT (9.8%),

Fe-BTC/PpPDA (3.8%), and Fe-BTC (5.9%) retained their peroxidase-like activity at pH 7.4 to a certain extent, which could be used for sensing. Further, unlike our present work where the sensing performance is demonstrated in neutral pH, a major proportion of MOF-based optical sensors have displayed peroxidase-like activity only in the mildly acidic range (pH 4–5), which limits the application of such materials in physiological systems.[29,31,83] Very few reports have demonstrated satisfactory sensing performance of MOFs-based optical sensors at neutral pH condition.[10] In the current work, an appreciable intrinsic peroxidase-like activity was exhibited by Fe-BTC/PEDOT > Fe-BTC > Fe-BTC/PpPDA in the decreasing order of activity (**Figure 4**) at neutral pH. Similar to the electrochemical response, in the colorimetric study, the best performance for detection of H_2O_2 at pH 7.4 was exhibited by Fe-BTC/PEDOT.
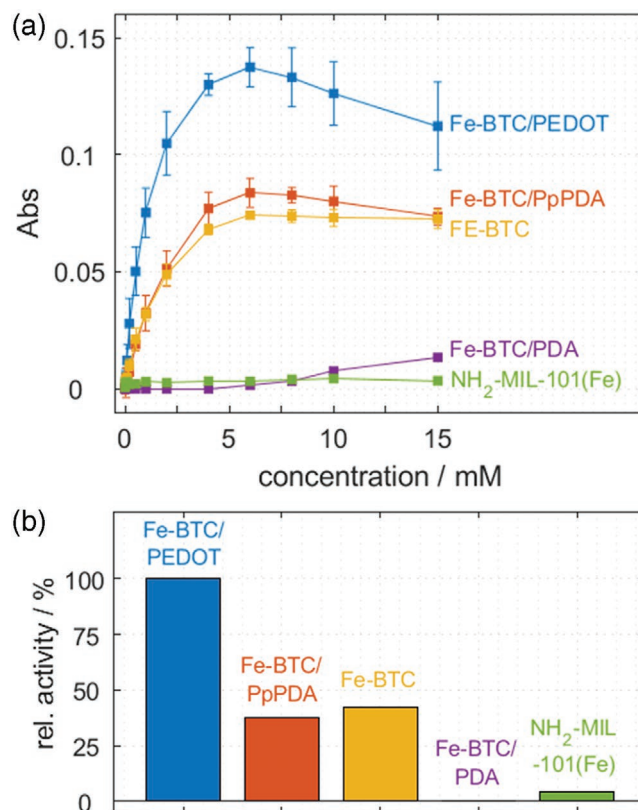

Figure 4. a) Response of Fe-BTC/PEDOT, Fe-BTC, Fe-BTC/PpPDA, Fe-BTC/PDA, and NH_2-MIL-101(Fe), to different concentrations of H_2O_2 (0 to 15×10^{-3} M) in PBS (1×10^{-3} M TMB, pH 7.4) at 652 nm. b) Relative activity of Fe-BTC/PEDOT, Fe-BTC/PpPDA, Fe-BTC, Fe-BTC/PDA, and NH_2-MIL-101(Fe) for 0.5×10^{-3} M H_2O_2 concentration. The highest activity was exhibited by Fe-BTC/PEDOT.

Akin to electrochemical sensors, in colorimetric sensors, the conducting polymer PEDOT is known to enhance the detection of analytes.[84–86] For example, an artificial peroxidase mimic composite comprising of Pd/PEDOT coaxial nanocables, was synthesized for the detection of H_2O_2. The high catalytic activity of the composite was attributed to the coaxial nanocable structure and the synergistic effect between Pd nanowires and the conducting polymer PEDOT.[86]

In the case of the Fe-BTC/PpPDA composite, it can be deduced from the colorimetric measurements that the presence of PpPDA did not impact the catalytic activity of Fe-BTC. Unlike Fe-BTC/PEDOT, Fe-BTC, and Fe-BTC/PpPDA, which exhibited a low detection limit for H_2O_2 (14- 23 µM), Fe-BTC/PDA and NH_2-MIL-101(Fe) displayed a very poor response for H_2O_2 sensing (**Table 2**) at pH 7.4. The sluggish activity of Fe-BTC/PDA composite for the detection of H_2O_2 can be attributed to the radical scavenging property of PDA. The oxidation of TMB is driven by $HO^{\bullet}$ produced during the reaction (Equations 5–9) and consumption of $HO^{\bullet}$ by PDA present in the Fe-BTC/PDA composite severely affects this oxidation. In the case of NH_2-MIL-101(Fe), its low peroxidase activity in comparison with Fe-BTC can be ascribed to the different crystalline structure, porosity, and functional groups present on the respective ligands in these two MOFs. In a recent study, a comparative investigation was carried out with two structurally identical MOFs (MOF-808FA and MOF-808). The superior catalytic activity of MOF-808 over MOF-808FA for colorimetric detection of H_2O_2 was attributed to the presence of –OH groups in MOF-808, which are substituted by coordinated formate groups in MOF-808FA.[10] In our current work, the presence of $–NH_2$ functionality in NH_2-MIL-101(Fe) can provide a possible explanation for its inactivity in comparison with Fe-BTC for colorimetric detection of H_2O_2.[44,47]

2.4. Comparing the Performance of MOFs/MOFs-Polymer Composites: Electrochemical versus Colorimetric Sensor

The study carried out in this work demonstrates the applicability of MOFs and MOFs/polymer composites as transducer materials for the electrochemical and colorimetric sensing of H_2O_2. Table S2 (Supporting Information) gives an overview of

Table 2. Colorimetric detection of H_2O_2: Comparison of sensing performance of metal-organic frameworks (MOFs) and MOFs/polymer composites with respect to various analytical parameters (derived from Figure 4a and Figure S9, Supporting Information). Similar to Fe-BTC/PDA, for NH_2-MIL-101(Fe) the relative activity is zero (for 0.5×10^{-3} M H_2O_2). In the case of NH_2-MIL-101(Fe), the slight increase in absorbance is due to the increase in turbidity of solution with the addition of H_2O_2 and not due to the oxidation of TMB (see Figure S10, Supporting Information).

	MOFs/MOFs composite	Linear range ($\times 10^{-3}$ M)	LOD ($\times 10^{-3}$ M)	Relative activity (for 0.5×10^{-3} M H_2O_2)
1	Fe-BTC/PEDOT	0.05–0.5	0.023	100%
2	Fe-BTC/PpPDA	0.2–2	0.018	38.4%
3	Fe-BTC	0.05–3	0.014	42%
4	Fe-BTC/PDA	6–20	3.52	0%
5	NH_2-MIL-101(Fe)	–	–	0%

the performance of some of the recent MOFs based artificial peroxidase sensors for the H_2O_2 detection (colorimetric and electrochemical techniques). In our study, for both electrochemical and colorimetric sensing platforms, the Fe-BTC/PEDOT composite emerged as the best candidate among the MOFs and MOFs/polymer composites studied. Compared to the Fe-BTC/PEDOT-based electrochemical sensor, the Fe-BTC/PEDOT-based colorimetric sensor exhibited a very low detection limit. The electrochemical sensor on the other hand, had a wider linear range, which extended to the higher limit compared to its colorimetric counterpart (Tables 1 and 2). Depending on the nature of the sample and type of analyte, a choice can be made between electrochemical and colorimetric methods of detection. For example, in combination with corresponding oxidase enzymes, Fe-BTC/PEDOT-based electrochemical biosensors can be employed for the detection of analytes such as glucose, uric acid, and cholesterol in blood. On the other hand, for detection of the aforementioned analytes at the cellular level (single cell or bacteria) and for immunoassays, where sensors must have much lower detection limits, we believe that the development of colorimetric biosensors, where the Fe-BTC/PEDOT composite can replace peroxidase, could be explored. It is noted that previous studies demonstrated that the crystallization of MOFs around enzymes or immobilization of biorecognition elements such as antibody, DNA, and aptamers on MOFs can increase the shelf life of these biomolecules and significantly extend their chemical and thermal stability.[87,88] As such, increasing the complexity of such composites seems like an exciting avenue to explore the development of highly sensitive biosensors.

3. Conclusion

We have investigated the activity of Fe-BTC, NH_2-MIL-101(Fe), and several MOFs/polymer composites consisting of Fe-BTC and PDA, PpPDA, or PEDOT as peroxidase mimics via electrochemical and optical methods. It was found that pristine Fe-BTC exhibited a considerable activity for the detection of H_2O_2 via both electrochemical and optical routes, while NH_2-MIL-101(Fe) showed negligible activity. This implies that the local environment around the redox-active iron site, porosity, and functionality on the ligand backbone likely plays a significant role in sensor performance. Next, we added polymers inside the pores of Fe-BTC to modulate its sensing properties. The MOFs/polymer composites were synthesized using a post-synthetic polymerization approach, resulting in the formation of polymer chains inside the cavities of Fe-BTC. Among the three MOFs/polymer composites, namely Fe-BTC/PDA, Fe-BTC/PpPDA, and Fe-BTC/PEDOT, only the composite containing PEDOT successfully improved the catalytic activity of Fe-BTC. This indicates that the incorporation of conducting polymers can be an effective approach to enhance the intrinsic peroxidase-like activity of MOFs. While the incorporation of PpPDA led to minimal change in the catalytic activity of Fe-BTC, PDA deteriorated the intrinsic peroxidase–like activity of Fe-BTC. We hypothesize that this observation likely results from the fact that PDA is a known radical scavenger.

To conclude, the present study demonstrates the potential of MOFs and MOFs/polymer composites in biosensing applica-

ADVANCED
SCIENCE NEWS
www.advancedsciencenews.com

ADVANCED
MATERIALS
TECHNOLOGIES
www.advmattechnol.de

tions, owed to their intrinsic peroxidase-like activity. We show that the addition of a conductive polymer inside the MOF pores, enhances the framework's sensing capabilities quite significantly, and hence, we believe this study provides new insight into the design of advanced sensing materials. Future investigations, meant to further develop structure-performance descriptors for such MOF-based sensors are needed. For instance, there is currently no understanding of how factors, such as the amount of polymer in the composite structure or the metal identity and its local environment influence the catalytic activity of MOFs based composites. Such studies will provide insights for further enhancing sensor performance. We envision, with the plethora of different MOFs and polymer building blocks to choose from, that one can use this type of chemistry as a platform for the design of new devices for different sensing applications.

4. Experimental Section

Materials: 1,3,5-benzenetricarboxylic acid (trimesic acid, 98%) was bought from ABCR GmbH and iron(III) chloride hexahydrate (97%) was bought from Alfa Aesar. p-Phenylenediamine (99%), dimethyl formamide, dimethyl aminoterephthalate, dopamine hydrochloride (99%), terephthalic acid (98%), Dulbecco's modified phosphate buffered saline, and H_2O_2 (30%) were purchased from Sigma-Aldrich. Anhydrous ethanol (99.8%) was bought from Acros. All chemicals were used without further purification. Carbon screen printed electrodes (SPE- 110, working electrode diameter: 4 mm) were purchased from DropSens. Deionized water was taken from an Ultra Clear purification system (EvoquaWater Technologies, Barsbüttel, Germany).

Synthesis of Fe-BTC: In a teflon autoclave (180 mL), iron(III) chloride hexahydrate (9.72 g), trimesic acid (3.36 g), and distilled water (120 mL) were mixed together. The reaction mixture was heated to 130 °C for 72 h. The reaction mixture was cooled down to room temperature and the orange solid was centrifuged at 7200 rpms followed by washing with water and methanol. The Fe-BTC powder was soxhleted with methanol for 24 h and then dried under vacuum overnight.

Synthesis of Fe-BTC/PpPDA: Fe-BTC/PpPDA was synthesized according to the established post-synthetic polymerization protocol.[16] Fe-BTC (1g) was activated overnight in a 2-neck round bottom flask (500 mL) overnight using a Schlenk line and an oil pump. The reaction vessel was then cooled down to room temperature and flushed with N_2. In a round bottom flask (250 mL), p-phenylenediamine (1.2 g) and anhydrous ethanol (200 mL) were loaded and capped with a septum. The reaction mixture was transferred to a steel cannula under nitrogen atmosphere and stirred for 1 h at 420 rpms. The reaction mixture was then exposed to air and heated to 50 °C for 24 h. The resulting brown powder was vacuum filtered and soxhleted with ethanol for 24 h. After purification, the sample was dried under vacuum overnight.

Synthesis of Fe-BTC/PDA: FeBTC/PDA was synthesized based on the previous report.[49] Fe-BTC (2 g) was activated overnight at 150 °C under vacuum in a 2-neck round bottom flask (500 mL) using a Schlenk line and an oil pump. The reaction vessel was cooled down to room temperature and keep under N_2 flow for 10 min. The sample was sealed under an inert atmosphere. N_2 purged anhydrous methanol solution (0.02 м, 400 mL) containing the as-prepared free base dopamine was transferred to the flask containing the activated Fe-BTC using a steel cannula and N_2. Due to polymerization, the orange powder turned dark purple over a period of 1 h. The reaction was stirred for 24 h at room temperature under an inert atmosphere. The reaction mixture was then vacuum filtered and washed with methanol and water. The purple powder was loaded into a double thickness Whatman cellulose extraction thimble to remove excess dopamine, followed by

Soxhlet extraction with methanol for 24 h under N_2. Finally, the sample was dried under vacuum at room temperature overnight.

Synthesis of Fe-BTC/PEDOT: Fe-BTC (1 g) was activated at 150 °C under vacuum using a 2-neck round bottom flask, a Schlenk line, and an oil pump overnight. After activation, the reaction vessel was cooled to room temperature and kept under N_2 flow. In a dry box, 3,4-ethylenedioxythiophene (0.75 mL) was mixed with anhydrous ethanol (150 mL) and sealed in a vessel. The ethanolic mixture was transferred to the reaction vessel via a steel cannula. The reaction was allowed to stir at room temperature for 1 h. Iodine (2 g) was then dissolved in ethanol (50 mL) and transferred to the reaction vessel. The reaction was allowed to stir at 420 rpm for 24 h. After completion of the reaction, the powder was separated from the reaction solution via centrifugation and washed with copious amounts of ethanol. Finally, the composite was dried at room temperature under vacuum overnight.

Synthesis of NH2-MIL-101(Fe): 2-Aminoterephthalic acid (225 mg, 1.25×10^{-3} м, 1 equiv.) and $FeCl_3 \cdot 6H_2O$ (675 mg, 2 equiv.) were each dissolved in dimethylformamide (DMF) (7.5 mL). Both solutions were mixed and the mixture was transferred to a Teflon line (30 mL) in a hydrothermal autoclave and heated for 24 h at 110 °C. After slow cooling of mixture at room temperature, the solid was separated from the solution through centrifugation. The solid was then washed three times with DMF (15 mL), three times with water (15 mL), and finally three times with ethanol (15 mL). After drying under vacuum at 150 °C overnight, powder consisting of crystals of NH2-MIL-101(Fe) was obtained.

Synthesis of PEDOT: The synthetic protocol was adapted from a previous report with minor modifications.[89] 3,4-Ethylenedioxythiophene (0.315 mL) was dispersed in HCl (50×10^{-3} м, 40 mL DI water +10 mL ethanol). The solution was sonicated for 30 min to improve the solubility of EDOT. Under constant stirring, APS (1.36 g 50 mL⁻¹ DI water) solution was added dropwise to the solution of EDOT monomer. The stirring was continued for 48 h at room temperature. The final product was washed with copious amount of ethanol (99.9%) and then dried in oven at 80 °C for 24 h.

Instruments: Mercury 3.6 crystallography software was used to generate simulated powder pattern. A Bruker D8 Discover system with a Cu Kα source (1.54056 Å) at 40 kV and 40 mA was used for powder X-ray diffraction. The primary and secondary optics slit were set to 12 and 9 mm with a NiO filter. The sample, which was grounded to fine powder, was loaded onto a 1 mm deep sample holder. The scan range was set from 1 to 80° (2760 steps) with 1 s exposure time per step.

The N_2 adsorption measurements were performed on a Micromeretics 3Flex. Samples (0.05–0.1 g) were activated at 125 °C under vacuum overnight. The samples were then filled back with argon, and transferred to the 3Flex adsorption analyzer. N_2 adsorption isotherms were recorded at 77 K with nitrogen and helium (99.999% purity). The surface areas (m²g⁻¹) were calculated using the BET (Brunaer–Emmet–Teller) method from the software.

Scanning electron microscopy images were recorded using JSM-6060LV, JEOL, Japan. BAL-TEC Med 020, LabMakelaar Benelux BV, the Netherlands was used to sputter coat the samples with gold (film thickness ≈7 nm) to limit electron-charging effect. Images were acquired with an acceleration voltage of 15 kV.

Electrochemical measurements were performed by a PalmSens4 potentiostat (PalmSens BV, Houten, The Netherlands) equipped with PSTrace 5.7 software. A three-electrode screen printed system integrated with glass was employed for cyclic voltammetry measurement (carbon working and auxiliary electrode and Ag/AgCl reference electrode). Before surface modifications, SPEs were cleaned with ethanol and DI water. Suspensions of MOFs and MOFs/polymer composites in PBS (1 mg 100 µL⁻¹, sonication for 15 min) were prepared. Prepared suspension (10 µL) was dropcasted on the working area of the SPE and dried at room temperature. Electrochemical impedance measurements were performed in PBS (pH 7.4) with 1×10^{-3} м Fe (CN)$_6^{3-/4-}$ redox couple from 100 kHz to 100 mHz with a voltage amplitude of 5 mV. Fresh stock solutions of H_2O_2 were made prior to every measurement and used within a day. All the measurements were carried out in PBS (pH 7.4).

UV-vis spectroscopy was recorded using Specord 210 (Analytik Jena, Germany). Stock solutions of TMB (20×10^{-3} M in DMSO), MOFs, and MOFs/polymer composites (2 mg mL^{-1} in PBS) were prepared. Fresh stock solution of H$_2$O$_2$ (1, 10, and 100×10^{-3} M) were made and used within a day. Different aliquots of H$_2$O$_2$ stock solutions were added to PBS, containing 50 µL each of TMB solution, and MOFs or MOFs/polymer composite solution. The final volume of reaction mixture was 1mL. For pH based measurements, pH of PBS was adjusted (4–7) using HCl (0.1 M). Prior to UV-vis measurements, the reaction mixture was allowed to incubate for 30 min at 37 °C.

Supporting Information

Supporting Information is available from the Wiley Online Library or from the author.

Conflict of Interest

The authors declare no conflict of interest.

Data Availability Statement

Research data are not shared.

[1] Y. Wei, Y. Zhang, Z. Liu, M. Guo, *Chem. Commun.* **2010**, *46*, 4472.
[2] T. Zhang, Y. Gu, C. Li, X. Yan, N. Lu, H. Liu, Z. Zhang, H. Zhang, *ACS Appl. Mater. Interfaces* **2017**, *9*, 37991.
[3] P. Pinyou, V. Blay, L. M. Muresan, T. Noguer, *Mater. Horiz.* **2019**, *6*, 1336.
[4] Y. Ou, A. M. Buchanan, C. E. Witt, P. Hashemi, *Anal. Methods* **2019**, *11*, 2738.
[5] Y. Lin, J. Ren, X. Qu, *Acc. Chem. Res.* **2014**, *47*, 1097.
[6] H. Wei, E. Wang, *Chem. Soc. Rev.* **2013**, *42*, 6060.
[7] Z. Li, W. Wang, H. Cao, Q. Zhang, X. Zhou, D. Wang, Y. Wang, S. Zhang, G. Zhang, C. Liu, Y. Zhang, R. Liu, J. Jiang, *Adv. Mater. Technol.* **2017**, *2*, 1770058.
[8] S. S. Menon, S. V. Chandran, A. Koyappayil, S. Berchmans, *ChemistrySelect* **2018**, *3*, 8319.
[9] J. Wang, W. Li, Y.-Q. Zheng, *Analyst* **2019**, *144*, 6041.
[10] H.-Q. Zheng, C.-Y. Liu, X.-Y. Zeng, J. Chen, J. Lü, R.-G. Lin, R. Cao, Z.-J. Lin, J.-W. Su, *Inorg. Chem.* **2018**, *57*, 9096.
[11] X.-L. Yang, X. Chen, G.-H. Hou, R.-F. Guan, R. Shao, M.-H. Xie, *Adv. Funct. Mater.* **2016**, *26*, 393.
[12] B. Rühle, E. Virmani, H. Engelke, F. M. Hinterholzinger, T. von Zons, B. Brosent, T. Bein, A. Godt, S. Wuttke, *Chem. - Eur. J.* **2019**, *25*, 6349.
[13] J. Zhou, G. Tian, L. Zeng, X. Song, X.-w. Bian, *Adv. Healthcare Mater.* **2018**, *7*, 1800022.
[14] V. Urbanová, K. Jayaramulu, A. Schneemann, Š. Kment, R. A. Fischer, R. Zbořil, *ACS Appl. Mater. Interfaces* **2018**, *10*, 41089.
[15] T. Kitao, Y. Zhang, S. Kitagawa, B. Wang, T. Uemura, *Chem. Soc. Rev.* **2017**, *46*, 3108.
[16] D. T. Sun, N. Gasilova, S. Yang, E. Oveisi, W. L. Queen, *J. Am. Chem. Soc.* **2018**, *140*, 16697.
[17] S. Yang, V. V. Karve, A. Justin, I. Kochetygov, J. Espín, M. Asgari, O. Trukhina, D. T. Sun, L. Peng, W. L. Queen, *Coord. Chem. Rev.* **2021**, *427*, 213525.
[18] K. Jiang, L. Zhang, Q. Hu, Q. Zhang, W. Lin, Y. Cui, Y. Yang, G. Qian, *Chem. - Eur. J.* **2017**, *23*, 10215.
[19] S. Yang, L. Peng, D. T. Sun, M. Asgari, E. Oveisi, O. Trukhina, S. Bulut, A. Jamali, W. L. Queen, *Chem. Sci.* **2019**, *10*, 4542.
[20] L. S. Xie, G. Skorupskii, M. Dincă, *Chem. Rev.* **2020**, *120*, 8037.
[21] J. Zhu, M. Xiao, Y. Zhang, Z. Jin, Z. Peng, C. Liu, S. Chen, J. Ge, W. Xing, *ACS Catal.* **2016**, *6*, 6335.
[22] B. Y. Guan, X. Y. Yu, H. B. Wu, X. W. Lou, *Adv. Mater.* **2017**, *29*, 1703614.
[23] C. Lu, T. Ben, S. Xu, S. Qiu, *Angew. Chem.* **2014**, *53*, 6454.
[24] W. Michida, A. Nagai, M. Sakuragi, K. Kusakabe, *Cryst. Res. Technol.* **2018**, *53*, 1700142.
[25] B. L.e Ouay, M. Boudot, T. Kitao, T. Yanagida, S. Kitagawa, T. Uemura, *J. Am. Chem. Soc.* **2016**, *138*, 10088.
[26] T. Wang, M. Farajollahi, S. Henke, T. Zhu, S. R. Bajpe, S. Sun, J. S. Barnard, J. S. Lee, J. D. W. Madden, A. K. Cheetham, S. K. Smoukov, *Mater. Horiz.* **2017**, *4*, 64.
[27] Z. Li, Y. Guo, X. Wang, W. Ying, D. Chen, X. Ma, X. Zhao, X. Peng, *Chem. Commun.* **2018**, *54*, 13865.
[28] W. Meng, S. Xu, L. Dai, Y. Li, J. Zhu, L. Wang, *Electrochim. Acta* **2017**, *230*, 324.
[29] X. Qi, H. Tian, X. Dang, Y. Fan, Y. Zhang, H. Zhao, *Anal. Methods* **2019**, *11*, 1111.
[30] L. Yang, C. Xu, W. Ye, W. Liu, *Sens. Actuators, B* **2015**, *215*, 489.
[31] B. Tan, H. Zhao, W. Wu, X. Liu, Y. Zhang, X. Quan, *Nanoscale* **2017**, *9*, 18699.
[32] J.-W. Zhang, H.-T. Zhang, Z.-Y. Du, X. Wang, S.-H. Yu, H.-L. Jiang, *Chem. Commun.* **2014**, *50*, 1092.
[33] J. Pan, M. Yang, L. Luo, A. Xu, B. Tang, D. Cheng, G. Cai, X. Wang, *ACS Appl. Mater. Interfaces* **2019**, *11*, 7338.
[34] I. del Agua, D. Mantione, U. Ismailov, A. Sanchez-Sanchez, N. Aramburu, G. G. Malliaras, D. Mecerreyes, E. Ismailova, *Adv. Mater. Technol.* **2018**, *3*, 1700322.
[35] H. Bae, D. Kim, M. Seo, I. K. Jin, S.-B. Jeon, H. M. Lee, S.-H. Jung, B. C. Jang, G. Son, K. Yu, S.-Y. Choi, Y.-K. Choi, *Adv. Mater. Technol.* **2019**, *4*, 1900151.
[36] J. P. Lowry, K. McAteer, S. S. El Atrash, A. Duff, R. D. O'Neill, *Anal. Chem.* **1994**, *66*, 1754.
[37] J. H. Koo, J.-K. Song, S. Yoo, S.-H. Sunwoo, D. Son, D.-H. Kim, *Adv. Mater. Technol.* **2020**, *5*, 2000407.
[38] M. Krogsgaard, V. Nue, H. Birkedal, *Chem. - Eur. J.* **2016**, *22*, 844.
[39] J. G. Rivera, P. B. Messersmith, *J. Sep. Sci.* **2012**, *35*, 1514.
[40] J. Rivnay, P. Leleux, M. Ferro, M. Sessolo, A. Williamson, D. A. Koutsouras, D. Khodagholy, M. Ramuz, X. Strakosas, R. M. Owens, C. Benar, J.-M. Badier, C. Bernard, G. G. Malliaras, *Sci. Adv.* **2015**, *1*, e1400251.

[41] M. Berggren, A. Richter-Dahlfors, *Adv. Mater.* **2007**, *19*, 3201.

[42] S. Zips, L. Grob, P. Rinklin, K. Terkan, N. Y. Adly, L. J. K. Weiß, D. Mayer, B. Wolfrum, *ACS Appl. Mater. Interfaces* **2019**, *11*, 32778.

[43] P. Horcajada, T. Chalati, C. Serre, B. Gillet, C. Sebrie, T. Baati, J. F. Eubank, D. Heurtaux, P. Clayette, C. Kreuz, J.-S. Chang, Y. K. Hwang, V. Marsaud, P.-N. Bories, L. Cynober, S. Gil, G. Férey, P. Couvreur, R. Gref, *Nat. Mater.* **2009**, *9*, 172.

[44] L. Sciortino, A. Alessi, F. Messina, G. Buscarino, F. M. Gelardi, *J. Phys. Chem. C* **2015**, *119*, 7826.

[45] M. Sanchez-Sanchez, I. de Asua, D. Ruano, K. Diaz, *Cryst. Growth Des.* **2015**, *15*, 4498.

[46] Y. Jia, Q. Mou, Y. Yu, Z. Shi, Y. Huang, S. Ni, R. Wang, Y. Gao, *Anal. Chem.* **2019**, *91*, 5217.

[47] B. Wu, X. Lin, L. Ge, L. Wu, T. Xu, *Chem. Commun.* **2013**, *49*, 143.

[48] A. D. S. Barbosa, D. Julião, D. M. Fernandes, A. F. Peixoto, C. Freire, B. de Castro, C. M. Granadeiro, S. S. Balula, L. Cunha-Silva, *Polyhedron* **2017**, *127*, 464.

[49] D. T. Sun, L. Peng, W. S. Reeder, S. M. Moosavi, D. Tiana, D. K. Britt, E. Oveisi, W. L. Queen, *ACS Cent. Sci.* **2018**, *4*, 349.

[50] Z. Zhang, X. Li, B. Liu, Q. Zhao, G. Chen, *RSC Adv.* **2016**, *6*, 4289.

[51] C. Ong, P. M. Bayley, O. Winther-Jensen, B. Winther-Jensen, *Polym. J.* **2013**, *45*, 391.

[52] B. Winther-Jensen, J. Chen, K. West, G. Wallace, *Macromolecules* **2004**, *37*, 5930.

[53] S.-S. Lin, M. D. Gurol, *Environ. Sci. Technol.* **1998**, *32*, 1417.

[54] B. Ensing, F. Buda, E. J. Baerends, *J. Phys. Chem. A* **2003**, *107*, 5722.

[55] W. G. Barb, J. H. Baxendale, P. George, K. R. Hargrave, *Trans. Faraday Soc.* **1951**, *47*, 462.

[56] H. L. Wiegand, C. T. Orths, K. Kerpen, H. V. Lutze, T. C. Schmidt, *Environ. Sci. Technol.* **2017**, *51*, 14321.

[57] G. Tachiev, J. A. Roth, A. R. Bowers, *Int. J. Chem. Kinet.* **2000**, *32*, 24.

[58] A. A. Karyakin, O. V. Gitelmacher, E. E. Karyakina, *Anal. Chem.* **1995**, *67*, 2419.

[59] C.-T. Chang, C.-Y. Lin, *RSC Adv.* **2016**, *6*, 67428.

[60] M. Vázquez-González, R. M. Torrente-Rodríguez, A. Kozell, W.-C. Liao, A. Cecconello, S. Campuzano, J. M. Pingarrón, I. Willner, *Nano Lett.* **2017**, *17*, 4958.

[61] J. Li, Y. Li, Y. Zhang, G. Wei, *Anal. Chem.* **2012**, *84*, 1888.

[62] M. I. Kim, Y. Ye, B. Y. Won, S. Shin, J. Lee, H. G. Park, *Adv. Funct. Mater.* **2011**, *21*, 2868.

[63] A. L.-T. Pham, F. M. Doyle, D. L. Sedlak, *Water Res.* **2012**, *46*, 6454.

[64] M. L. Kremer, *Trans. Faraday Soc.* **1963**, *59*, 2535.

[65] K. Cinková, M. Clark, S. V. Sokolov, C. Batchelor-McAuley, Ľ. Švorc, R. G. Compton, *Electroanalysis* **2017**, *29*, 1006.

[66] W. Chen, S. Cai, Q.-Q. Ren, W. Wen, Y.-D. Zhao, *Analyst* **2012**, *137*, 49.

[67] E. Shi, X. Zou, J. Liu, H. Lin, F. Zhang, S. Shi, F. Liu, G. Zhu, F. Qu, *Dalton Trans.* **2016**, *45*, 7728.

[68] T.-Y. Huang, C.-W. Kung, Y.-T. Liao, S.-Y. Kao, M. Cheng, T.-H. Chang, J. Henzie, H. R. Alamri, Z. A. Alothman, Y. Yamauchi, K.-C. Ho, K. C.-W. Wu, *Adv. Sci.* **2017**, *4*, 1700261.

[69] B. Li, H. Lopez-Beltran, C. Siu, K. H. Skorenko, H. Zhou, W. E. Bernier, M. S. Whittingham, W. E. Jones, *ACS Appl. Energy Mater.* **2020**, *3*, 1559.

[70] S. Mukhopadhyay, O. Basu, R. Nasani, S. K. Das, *Chem. Commun.* **2020**, *56*, 11735.

[71] A. P. Mártire, G. M. Segovia, O. Azzaroni, M. Rafti, W. Marmisollé, *Mol. Syst. Des. Eng.* **2019**, *4*, 893.

[72] F. Zheng, Z. Zhang, C. Zhang, W. Chen, *ACS Omega* **2020**, *5*, 2495.

[73] K.-Y. Ju, Y. Lee, S. Lee, S. B. Park, J.-K. Lee, *Biomacromolecules* **2011**, *12*, 625.

[74] L. Panzella, G. Gentile, G. D'Errico, N. F. Della Vecchia, M. E. Errico, A. Napolitano, C. Carfagna, M. d'Ischia, *Angew. Chem.* **2013**, *52*, 12684.

[75] Z. Wang, F. Tang, H. Fan, L. Wang, Z. Jin, *Langmuir* **2017**, *33*, 5938.

[76] T. Liu, K. C. Kim, B. Lee, Z. Chen, S. Noda, S. S. Jang, S. W. Lee, *Energy Environ. Sci.* **2017**, *10*, 205.

[77] E. P. Randviir, C. E. Banks, *Anal. Methods* **2013**, *5*, 1098.

[78] L. Shen, R. Liang, M. Luo, F. Jing, L. Wu, *Phys. Chem. Chem. Phys.* **2015**, *17*, 117.

[79] F. Chen, D. Bai, X. Wang, Y. He, *Inorg. Chem. Front.* **2017**, *4*, 960.

[80] Z.-W. Mo, H.-L. Zhou, J.-W. Ye, D.-D. Zhou, P.-Q. Liao, W.-X. Zhang, J.-P. Zhang, *Cryst. Growth Des.* **2018**, *18*, 2694.

[81] P. V. Dau, K. K. Tanabe, S. M. Cohen, *Chem. Commun.* **2012**, *48*, 9370.

[82] M. Almáši, V. Zeleňák, P. Palotai, E. Beňová, A. Zeleňáková, *Inorg. Chem. Commun.* **2018**, *93*, 115.

[83] C. Song, W. Ding, H. Liu, W. Zhao, Y. Yao, C. Yao, *New J. Chem.* **2019**, *43*, 12776.

[84] X. Xu, W. Wang, B. Sun, X. Zhang, R. Zhao, C. Wang, *Materials* **2018**, *11*, 2084.

[85] M. Chi, Y. Zhu, Z. Yang, M. Gao, S. Chen, N. Song, C. Wang, X. Lu, *Nanotechnology* **2017**, *28*, 296704.

[86] M. Chi, G. Nie, Y. Jiang, Z. Yang, Z. Zhang, C. Wang, X. Lu, *ACS Appl. Mater. Interfaces* **2016**, *8*, 1041.

[87] C. Wang, J. Gao, H. Tan, *ACS Appl. Mater. Interfaces* **2018**, *10*, 25113.

[88] D. J. Bell, M. Wiese, A. A. Schönberger, M. Wessling, *Angew. Chem., Int. Ed.* **2020**, *59*, 16047.

[89] N. Paradee, A. Sirivat, *Polym. Int.* **2014**, *63*, 106.